ACS Photonics

Article

pubs.acs.org/journal/apchd5

Enhanced Efficiency in Dye-Sensitized Solar Cells with Shape-Controlled Plasmonic Nanostructures

Holly F. Zarick,[†] Olivia Hurd,[‡] Joseph A. Webb,[†] Chanse Hungerford,[§] William R. Erwin,[†] and Rizia Bardhan*,[†]

[†]Department of Chemical and Biomolecular Engineering, [‡]Department of Mechanical Engineering, and [§]Department of Electrical Engineering and Computer Science, Vanderbilt University, Nashville, Tennessee 37235, United States

Supporting Information

ABSTRACT: In this work, we demonstrate enhanced light harvesting in dye-sensitized solar cells (DSSCs) with gold nanocubes of controlled shape. Silica-coated nanocubes (Au@SiO_2 nanocubes) embedded in the photoanodes of DSSCs had a power conversion efficiency of 7.8% relative to 5.8% of reference (TiO_2 only) devices, resulting in a 34% improvement in DSSC performance. Photocurrent behavior and incident photon to current efficiency spectra revealed that device performance is controlled by the particle density of Au@SiO_2 nanocubes and monotonically decreases at very high nanocube concentration. Finite difference time domain simulations suggest that, at the 45 nm size regime, the nanocubes predominantly absorb incident light, giving rise to the lightning rod effect, which results in intense electromagnetic fields at the edges and corners. These intense fields increase the plasmonic molecular coupling, amplifying the carrier generation and DSSC efficiency.

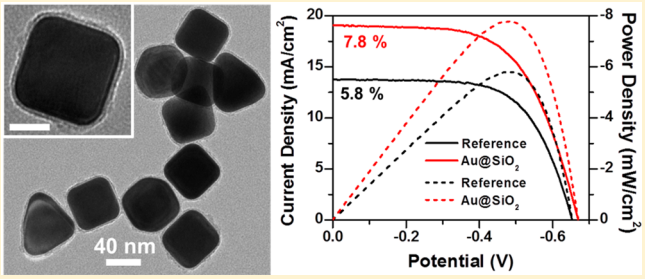

KEYWORDS: *plasmon-enhanced, dye-sensitized solar cells, gold nanoparticles, nanocubes, photovoltaics, plasmon−molecule coupling*

Dye-sensitized solar cells (DSSCs) have rapidly emerged as an appealing alternative to silicon photovoltaics due to the low processing costs and inexpensive constituent materials. Recent efforts to improve power conversion efficiencies (PCEs) have focused on the synthesis of panchromatic sensitizers, such as porphyrins, with enhanced light-harvesting characteristics in the 600−900 nm wavelength range.[1] While effective, the overall PCE of these sensitizers is often lower than the best performing ruthenium dyes due to their reduced incident photon to current efficiency (IPCE) at shorter wavelengths. In addition to organic sensitizers, semiconductor quantum dots have also been utilized to enhance light absorption in solar cells.[2] However, new sensitizers often alter the energy band positions relative to the conduction band of TiO_2 and are incompatible with the redox potential of the electrolyte.[3,4] Misaligned band energies result in poor charge separation and high recombination, lowering the overall device efficiency. Other strategies to augment light absorption have focused on increasing the thickness or changing the morphology of the photoanodes[5,6] and adding scattering layers or back reflectors.[7,8] Whereas these approaches have resulted in incremental enhancements in PCE, the higher materials and fabrication costs associated with thick film solar cells have outweighed the benefits. Alternative approaches are hence imperative to increase the overall light trapping in DSSCs and enhance the PCE without altering the material or electronic properties of sensitizers.

Metal nanostructures integrated with DSSCs can significantly amplify the light-harvesting characteristics of sensitizing molecules without affecting their chemical functionalities.[9−13] Following photoexcitation, metal nanostructures couple incident photons to conduction band electrons, generating surface plasmon resonances (SPRs). These SPRs give rise to light scattering into the nanoparticle far field, as well as generation of electromagnetic near fields, which decay exponentially within tens of nanometers from the particle surface.[14] By effectively manipulating these near-field and far-field properties, a range of technological applications have been realized, including chemical and biological sensing,[15] nanomedicine,[16] solar devices,[17−19] and photodetectors. The absorption and scattering efficiencies are governed by both the nanostructure size and shape. Nanostructures >100 nm in size primarily scatter light, whereas smaller nanostructures predominantly absorb light. Unlike spherical nanoparticles, isotropic and anisotropic plasmonic nanostructures with sharp edges and corners generate intense fields localized at the corners and behave as "nanosized light concentrators".[20,21] Such shape-controlled nanostructures, when coupled with sensitizing molecules in a DSSC, give rise to three distinct phenomena: (1) nanostructures capture solar energy and scatter light, which is reabsorbed by the dye monolayer, increasing the total light harvested by the dye; (2) nanostructures function as antennas, coupling the plasmonic near field to the optical absorption of the sensitizer, thereby

Received: March 20, 2014
Published: August 27, 2014

increasing the total absorption cross-section; and (3) nanostructures convert incident photons to "hot" electrons, which are rapidly injected into the conduction band of TiO_2, amplifying the number of carriers available for photocurrent generation.[32,33] The strongest plasmon−molecule coupling is achieved when the absorption of the molecules overlaps with the nanostructure plasmon resonance, a phenomenon that has been actively harnessed in surface-enhanced spectroscopies.[22−24]

Whereas metal-enhanced DSSCs have largely focused on spherical nanostructures,[10,12,13,25−28] here we demonstrate the use of gold (Au) nanocubes of controlled geometry and dimensions to enable plasmonic enhancement of solar cells. Relative to their spherical counterparts, a cubic morphology (1) has two times higher absorption and extinction efficiency and three times higher scattering efficiency (Figure S1), (2) has about two times larger surface area, which suggests more dye molecules will be enhanced for a given DSSC area (see Supporting Information for details), and (3) facilitates a higher concentration of charges localized at the corners and edges, giving rise to larger electromagnetic fields due to the quasi-static lightning-rod effect.[21,29,30] These confined fields can be used as a secondary light source to promote optical interactions with vicinal molecules and materials. In this work, we have coated the Au nanocubes in a 3−5 nm uniform layer of silica ($Au@SiO_2$) and incorporated them into the photoanodes of DSSCs. We observed that 1.8 wt % $Au@SiO_2$ nanocubes in photoanodes resulted in a 34% increase in the PCE of the device, and we note that device performance is driven entirely by an improvement in short-circuit current density. By varying the concentration of $Au@SiO_2$ nanocubes in DSSCs, we find a systematic dependence of nanocube wt % on device efficiency. IPCE measurements demonstrate that the improvement in device performance is attributed to the enhanced light harvesting in the visible region of the spectrum due to direct coupling of Au nanocube plasmons with N719, ditetrabutylammonium *cis*-bis(isothiocyanato)bis(2,2′-bipyridyl-4,4′-dicarboxylato)ruthenium(II), dye molecules.

Au nanocubes of ∼45 ± 3 nm edge length (Figure S2) were synthesized following a procedure previously described,[31] by a seed-mediated growth process with cetyltrimethylammonium bromide (CTAB) ligands as a shape-directing agent in aqueous media. We calculated the absorption and scattering efficiencies of rounded-corner nanocubes of a range of sizes (Figure S3). On the basis of our calculations, at the 45−60 nm size range, absorption to light scattering ratios are optimal, and hence this size was chosen. Before integrating the nanocubes in DSSC anodes, they were coated with a thin, 3−5 nm, layer of silica, generating $Au@SiO_2$ nanocubes (Figure 1a).[32] The silica layer serves several purposes. Since metals are electron scavengers, the silica spacer provides electrical isolation, minimizing recombination of electron−hole (e^-/h^+) pairs on the surface of the metal.[12] The silica layer protects the metal from the corrosive iodide/triiodide (I^-/I_3^-) liquid electrolyte. Finally, the silica layer also provides thermal stability to the nanocubes, reducing Ostwald ripening during the 500 °C annealing processes necessary for DSSC fabrication. A ∼3−5 nm silica layer is adequate in providing thermal and chemical stability to the nanocubes without detrimentally dampening the electromagnetic fields surrounding the nanocube surface. Thicker layers of silica (>10 nm) not only result in a red-shift of the plasmon resonance due to the higher refractive index of silica, but also shield the electron oscillation on the metal, causing

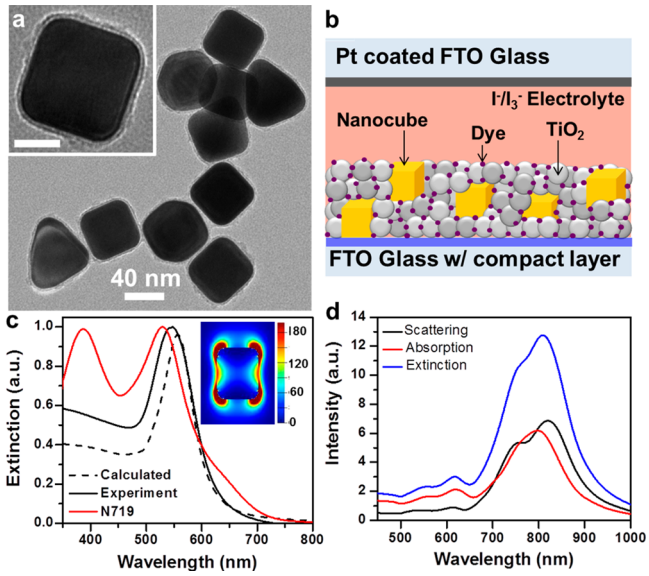

Figure 1. (a) Low-magnification TEM micrograph of $Au@SiO_2$ nanocubes and high-magnification image provided in the inset. The scale bar is 20 nm in the inset. (b) Schematic representation of plasmon-enhanced DSSCs showing nanocubes embedded within the N719-sensitized mesoporous TiO_2 layer with I^-/I_3^- liquid electrolyte. (c) Normalized experimental (solid black) and calculated (dashed black) extinction spectra of rounded-corner Au nanocubes in aqueous media with the electromagnetic intensity profile, $\langle E^2/E_0^2\rangle$, in the inset. The absorption spectrum of N719 is also shown (red) to compare the peak position of N719 with Au nanocubes. (d) Calculated absorption, scattering, and extinction spectra of 45 nm edge length Au nanocubes in anatase TiO_2 surrounding media.

plasmon dampening.[33] $Au@SiO_2$ nanocubes were integrated in DSSC photoanodes by mixing a concentrated colloidal solution with 20 nm TiO_2 nanoparticle paste to form a homogeneous mixture. The mixture was deposited on fluorine-doped tin oxide (FTO) glass substrates by doctor blading and sintered to convert the amorphous TiO_2 to its crystalline anatase phase. The nanocube-incorporated TiO_2 active layer was then sensitized with dye. FTO glass with a thin layer of Pt served as the cathode, and an I^-/I_3^- redox couple based liquid electrolyte enabled electron transport between the electrodes. A schematic representation of the plasmon-enhanced DSSC is illustrated in Figure 1b. The optical characteristics of the nanocubes showed good overlap with the absorption spectrum of the N719 sensitizer (Figure 1c). Finite difference time domain (FDTD) simulations were performed to predict the absorption and scattering contributions of the nanocubes and overall extinction behavior. The calculated extinction spectrum (Figure 1c) of the nanocubes (555 nm) is slightly red-shifted from the experimental spectrum (548 nm). This shift is due to the heterogeneity in the reaction mixture attributed to the presence of both rounded-corner nanocubes and truncated nanocubes. Detailed particle distribution analysis is provided in the Supporting Information (Figure S4). As expected, the sub-50 nm size regime of the nanocubes results in a very low albedo, i.e., ratio of scattering to total extinction (Figure 1d), suggesting that nanocube-enhanced PCE of DSSCs occurs via near-field coupling with the dye molecules. The electromagnetic intensity profile, $\langle E^2/E_0^2\rangle$, at the plasmon resonance peak of the Au nanocubes (Figure 1d inset) illustrates intense near fields localized at the edges and corners of the nanocubes. We note that, due to the high absorption to scattering ratio of

dx.doi.org/10.1021/ph500281v | ACS Photonics 2014, 1, 806−811

$Au@SiO_2$ nanocubes, we chose to embed the nanocubes within the mesoporous TiO_2 layer of the photoanodes (Figure 1a) to enhance the overall optical absorption of the devices. Plasmonic nanostructures designed by lithographic approaches have been incorporated into DSSCs as back reflectors on the conductive substrate[18,34] or on the counter electrode surface,[35] both of which enhance the overall device performance by forward light scattering with minimal contribution from near-field coupling. While effective, forward scattered light may not effectively couple with all of the sensitizer molecules within the ~10 μm mesoporous layer; our strategy therefore focused on homogeneous mixing of the nanocubes within the TiO_2 layer to maximize proximity to sensitizer molecules.

To understand the mechanism of plasmonic enhancement of DSSCs, an energy diagram showing the mechanistic processes of DSSCs incorporated with nanostructured Au is demonstrated in Figure 2. Upon illumination, Au nanocubes

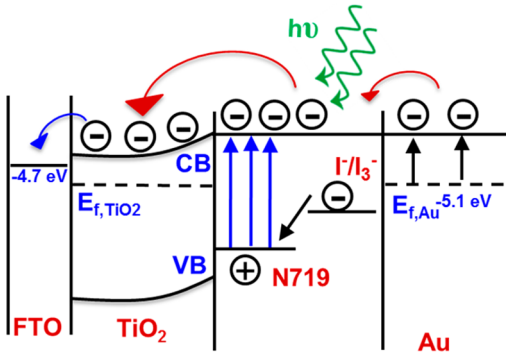

Figure 2. Energy diagram describing how the molecular coupling between plasmonic nanostructure and sensitizer results in enhanced absorption by N719, generating more electrons that transfer from the LUMO of the dye to the conduction band of TiO_2.

preferentially absorb (with some scattering) incident light, generating confined electromagnetic fields on their surface. The vicinal sensitizer molecules couple with the intense plasmonic near field, using it as a secondary light source. This plasmon−molecular coupling results in enhanced light absorption by the dye molecules, augmenting the number of electron−hole pairs produced in the sensitizer. This subsequently results in a larger number of electrons transferring from the lowest unoccupied molecular orbital (LUMO) of the sensitizer to the conduction band of TiO_2. A larger carrier density increases the overall short-circuit current density of the DSSCs.

The optical absorption spectrum of the mesoporous TiO_2 sensitized with N719 is significantly enhanced with $Au@SiO_2$ nanocubes incorporated in the photoanodes (Figure 3a). Spectra are shown for the best performing devices containing an optimized concentration of 1.8 wt % $Au@SiO_2$ nanocubes. We also show the absorbance in total percentage units in the Supporting Information (Figure S5) to demonstrate the amount of light absorbed in the devices. The absorption enhancement in photoanodes incorporated with nanocubes (Figure 3b), obtained by normalizing to a reference, shows strong improvement in light harvesting throughout the visible and near-infrared. Particularly, a three-fold enhancement in the 400−600 nm region is attributed to dipole−dipole coupling of nanocubes and dye molecules. We also note that a 4−12 times absorption enhancement is also observable in the 600−800 nm region, attributable to a red-shift of the plasmon resonance of

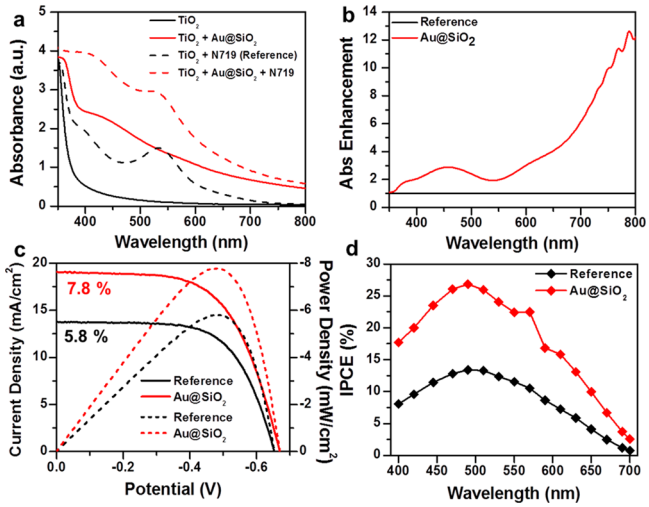

Figure 3. (a) Optical absorption spectra of mesoporous TiO_2 before and after sensitizing with N719 and embedded with $Au@SiO_2$ nanocubes. The sample TiO_2 + N719 is referred to as "Reference", and the sample with TiO_2 + $Au@SiO_2$ + N719 is referred to as "$Au@SiO_2$" in (b), (c), and (d). (b) Absorption enhancement after embedding $Au@SiO_2$ nanocubes in the photoanode. A strong improvement in light harvesting is observed throughout the visible and near-infrared. (c) Current density (solid lines) and power density (dashed lines) curves of the DSSCs with ($Au@SiO_2$) and without (Reference) nanocubes. Corresponding incident photon to current efficiency (IPCE) curves are shown in (d). All plasmon-enhanced data are shown for the best performing devices with an optimized concentration of 1.8 wt % $Au@SiO_2$ nanocubes.

$Au@SiO_2$ nanocubes when embedded in the high refractive index (n = 2.55) of the TiO_2 mesoporous layer (Figure 1d), as well as some clustering of the nanocubes within the TiO_2 layer. In addition to the red-shift, both clustering of nanocubes and a high dielectric constant surrounding media also increase the overall light-scattering ability of the $Au@SiO_2$ nanocubes, improving the optical path length of the DSSCs and enhancing the device efficiency.[17] The PCEs of reference and plasmon-enhanced DSSCs of equivalent area of 0.12 cm^2 were examined under AM 1.5 illumination and received one sun (100 mW/cm^2) of power. The best performing reference and $Au@SiO_2$ nanocube-incorporated devices (Figure 3c) had PCEs of 5.8% and 7.8%, respectively, i.e., a 34% increase in PCE with plasmonic enhancement of DSSCs. IPCE measurements for these devices were performed to investigate the spectral response of DSSCs (Figure 3d) and to examine the light-harvesting characteristics of the plasmon-enhanced devices. A supercontinuum white light laser coupled with an acousto-optical tunable filter was used to modulate the wavelengths from 400 to 700 nm. While the shape of IPCE spectra of plasmon-enhanced and reference devices are similar, the nanocube-incorporated devices showed a remarkable increase across the visible spectrum, specifically in the 450−550 nm range, overlapping with the plasmon resonance of $Au@SiO_2$ nanocubes. The IPCE spectra correspond well with the absorption spectra (Figure 3a), supporting that the nanocubes promote light trapping in the DSSCs. Enhancement in IPCE of nanocube-enhanced DSSCs relative to the reference is shown in Figure S6.

To further understand the light-harvesting capabilities of $Au@SiO_2$ nanocubes, the optimum concentration of the nanocubes was found by varying the particle density of

dx.doi.org/10.1021/ph500281v | ACS Photonics 2014, 1, 806−811

nanocubes from 0.6 to 4.47 wt % in the TiO_2 active layer. The absorption spectra of nanocube-embedded anodes are shown in Figure 4a. For clarity, only selected concentrations are shown here; detailed spectra of all of the particle densities are shown in the Supporting Information (Figure S7). The optical absorption gradually increases across the entire visible spectrum with increasing nanocube concentration, indicating a stronger coupling between nanocube plasmons and dye molecules. At very high particle density of Au@SiO_2 nanocubes (>2.95 wt %) in the TiO_2 active layer, we observe a strong red-shift in the optical absorption, which may be attributable to an increase in nanocube clustering at such high concentrations. The PCEs of the plasmon-enhanced DSSCs were examined under the same conditions as described above. Photocurrent spectra for select devices are shown in Figure 4b (see Figure S8 for all the concentrations). IPCE measured in the 400−700 nm wavelength range (Figure 4c and Figure S9 for all concentrations) follows a similar trend to that observed in the photocurrent spectra (Figure 4b); IPCE is enhanced across the visible spectrum and reaches a maximum for 1.8 wt % Au@SiO_2 nanocube concentration and then decreases with increasing concentration. The IPCE spectral characteristics correspond well to the absorbance spectra of the N719-sensitized photoanodes, and all show maximum enhancements in the 450−550 nm range, where the plasmon resonance peak of the nanocubes occurs. We note that all IPCE spectra show an enhancement relative to the reference (Figure S9), which suggests that even at the high particle densities of Au@SiO_2 nanocubes, plasmonic light trapping still occurs in these devices.

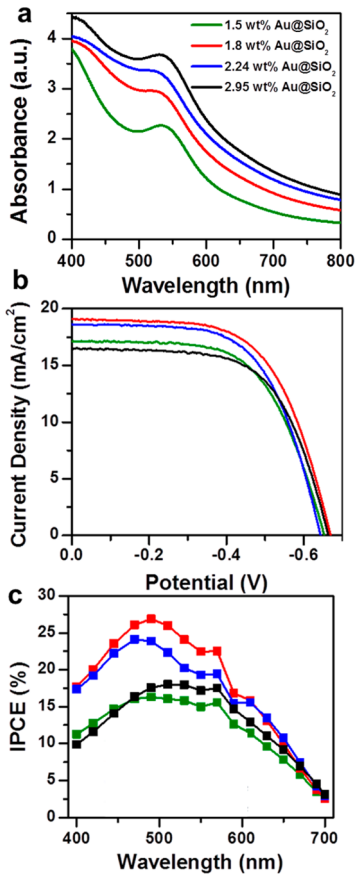

Figure 4. (a) Optical absorption spectra of N719-sensitized mesoporous TiO_2 with varied particle density of Au@SiO_2 nanocubes embedded in the photoanodes. (b) Corresponding current density spectra of the devices. (c) % IPCE of the same devices as a function of excitation wavelength.

The detailed device performances of reference (non-enhanced) and plasmon-enhanced devices for all of the particle densities are shown in Figure 5 and also provided in Table S2.

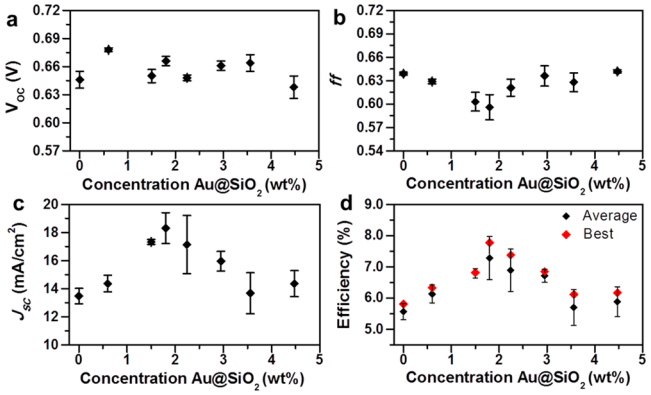

Figure 5. Open-circuit voltage (a), fill factor (b), short-circuit current density (c), and both average and best power conversion efficiency from five devices are shown as a function of Au@SiO_2 nanocube particle density (wt %). The nanocube concentration was varied between 0.6 and 4.47 wt %.

The open-circuit voltage (V_{oc}) and fill factor (FF) of the devices are almost equivalent (Figure 5a,b) with a significant increase in the short-circuit current density (J_{sc}) of the Au@SiO_2 nanocube-incorporated devices (Figure 5c). This indicates that the observed plasmonic enhancements in DSSC efficiency are not due to any changes in the electrochemical properties, but rather due to improved light harvesting in DSSCs, resulting in an increased J_{sc}. The best efficiencies obtained for the DSSCs (Figure 5d) indicate that a maximum PCE of 7.8% is achieved for plasmon-enhanced DSSCs with 1.8 wt % of nanocubes. We note that even at a low concentration of 0.6 wt % of Au@SiO_2 nanocubes incorporated in the photoanodes, a 6.33% PCE is obtained, i.e., a 9% increase in efficiency relative to the reference device (5.8% PCE). Both best and average PCEs of plasmon-enhanced DSSCs reach a maximum at 1.8 wt % of nanocubes, then monotonically decrease with further increases in concentration, and finally level off at 4.47 wt % of nanocubes in the active layer. This decrease in device performance at high particle density of Au@SiO_2 nanocubes may be attributable to three phenomena: (1) the high concentration of metal increases electron−hole recombination, decreasing the number of carriers available for photocurrent generation; (2) large volume of nanocubes results in the loss of absorbing dye volume; and (3) the high nanocube density and interparticle interaction between adjacent nanocubes may result in light to heat conversion by electron−phonon coupling. The dissipation of this heat results in an increase in phonon density, which consequently reduces the number of carriers available for photocurrent generation, decreasing device efficiency.[13,25] We have also provided a table in the Supporting Information (Table S2) with examples from the literature of other plasmon-enhanced work on DSSCs and how the efficiencies compare to our work.

In summary, we employed shape-controlled gold nanocubes coated in a thin, uniform layer of silica, Au@SiO_2 nanocubes, in

dx.doi.org/10.1021/ph500281v | ACS Photonics 2014, 1, 806−811

the photoanodes of DSSCs and observed a 34% increase in efficiency relative to the reference (nonenhanced) devices. By varying the particle density, we observed a systematic dependence of device performance on the nanocube concentration; maximum enhancement was achieved with a 1.8 wt % concentration of nanocubes. The 7.8% PCE achieved with the best performing plasmon-enhanced DSSC is attributed to a combination of intense electromagnetic fields confined at the corners and edges of the nanocubes, due to the lightning-rod effect, and nanocube scattering into the far field. Both phenomena give rise to plasmonic−molecular coupling and enhanced light absorption by the sensitizer. The enhanced light-harvesting characteristics of DSSCs integrated with nanocubes will ultimately enable the design of high-efficiency thin-film solar cells with a thickness of <500 nm with lower costs and better stability. The intrinsic properties of such shape-controlled metal nanostructures make them appealing for a range of optoelectronic devices beyond DSSCs, such as Si photovoltaics, organic solar cells, perovskite solar cells, and photodetectors.

METHODS

Detailed experimental methods are provided in the Supporting Information.

ASSOCIATED CONTENT

Supporting Information

Experimental methods, additional calculated spectra of nanocubes and other shapes, additional absorption, photocurrent, and IPCE data, SEM and TEM images of Au nanocubes, SEM image of DSSC, detailed Table with plasmon-enhanced efficiency achieved with other nanostructures, Table with Voc, FF, Jsc, and η achieved in this work, are provided. This material is available free of charge via the Internet at http://pubs.acs.org.

AUTHOR INFORMATION

Corresponding Author

*E-mail: rizia.bardhan@vanderbilt.edu.

Notes

The authors declare no competing financial interest.

ACKNOWLEDGMENTS

This work was supported by NSF EPSCOR (NSF EPS1004083) and NSF BRIGE (EEC 1342185). H.F.Z. acknowledges support from the Department of Education for a Graduate Assistance in Areas of National Need (GAANN) Fellowship under grant number P200A090323. The authors acknowledge facilities support from Oak Ridge National Laboratory user proposal CNMS 2013-287. The authors also acknowledge Prof. Cary Pint for helpful discussions.

REFERENCES

(1) Yella, A.; Lee, H.-W.; Tsao, H. N.; Yi, C.; Chandiran, A. K.; Nazeeruddin, M. K.; Diau, E. W.-G.; Yeh, C.-Y.; Zakeeruddin, S. M.; Grätzel, M. Porphyrin-Sensitized Solar Cells with Cobalt (II/III)-Based Redox Electrolyte Exceed 12% Efficiency. *Science* **2011**, *334*, 629−634.

(2) Beard, M. C.; Luther, J. M.; Semonin, O. E.; Nozik, A. J. Third Generation Photovoltaics Based on Multiple Exciton Generation in Quantum Confined Semiconducters. *Acc. Chem. Res.* **2013**, *46*, 1252−1260.

(3) Chen, C.-Y.; Wang, M.; Li, J.-Y.; Pootrakulchote, N.; Alibabaei, L.; Ngoc-le, C.-h.; Decoppet, J.-D.; Tsai, J.-H.; Gratzel, C.; Wu, C.-G.; Zakeeruddin, S. M.; Gratzel, M. Highly Efficient Light-Harvesting Ruthenium Sensitizer for Thin-Film Dye-Sensitized Solar Cells. *ACS Nano* **2009**, *3*, 3103−3109.

(4) Kamat, P. V. Boosting the Efficiency of Quantum Dot Sensitized Solar Cells through Modulation of Interfacial Charge Transfer. *Acc. Chem. Res.* **2012**, *45*, 1906−1915.

(5) Kim, K. S.; Song, H.; Nam, S. H.; Kim, S.-M.; Jeong, H.; Kim, W. B.; Jung, G. Y. Fabrication of an Efficient Light-Scattering Functionalized Photoanode Using Periodically Aligned ZnO Hemisphere Crystals for Dye-Sensitized Solar Cells. *Adv. Mater.* **2012**, *24*, 792−798.

(6) Feng, X.; Zhu, K.; Frank, A. J.; Grimes, C. A.; Mallouk, T. E. Rapid Charge Transport in Dye-Sensitized Solar Cells Made from Vertically Aligned Single-Crystal Rutile TiO_2 Nanowires. *Angew. Chem.* **2012**, *124*, 2781−2784.

(7) Roy, P.; Kim, D.; Lee, K.; Spiecker, E.; Schmuki, P. TiO_2 Nanotubes and their Application in Dye-Sensitized Solar Cells. *Nanoscale* **2010**, *2*, 45−59.

(8) Han, S.-H.; Lee, S.; Shin, H.; Jung, H. S. A Quasi-Inverse Opal Layer Based on Highly Crystalline TiO_2 Nanoparticles: A New Light-Scattering Layer in Dye-Sensitized Solar Cells. *Adv. Energy Mater.* **2011**, *1*, 546−550.

(9) Gangishetty, M. K.; Lee, K. E.; Scott, R. W.; Kelly, T. L. Plasmonic Enhancement of Dye Sensitized Solar Cells in the Red-to-Near-Infrared Region Using Triangular Core-Shell Ag@SiO_2 Nanoparticles. *ACS Appl. Mater. Interfaces* **2013**, *5*, 11044−11051.

(10) Chen, P.-Y.; Dang, X.; Klug, M. T.; Qi, J.; Dorval Courchesne, N.-M.; Burpo, F. J.; Fang, N.; Hammond, P. T.; Belcher, A. M. Versatile Three-Dimensional Virus-Based Template for Dye-Sensitized Solar Cells with Improved Electron Transport and Light Harvesting. *ACS Nano* **2013**, *7*, 6563−6574.

(11) Chang, S.; Li, Q.; Xiao, X.; Wong, K. Y.; Chen, T. Enhancement of Low Energy Sunlight Harvesting in Dye-Sensitized Solar Cells Using Plasmonic Gold Nanorods. *Energy Environ. Sci.* **2012**, *5*, 9444−9448.

(12) Brown, M. D.; Suteewong, T.; Kumar, R. S.; D'Innocenzo, V.; Petrozza, A.; Lee, M. M.; Wiesner, U.; Snaith, H. J. Plasmonic Dye-Sensitized Solar Cells Using Core-Shell Metal-Insulator Nanoparticles. *Nano Lett.* **2011**, *11*, 438−445.

(13) Dang, X.; Qi, J.; Klug, M. T.; Chen, P. Y.; Yun, D. S.; Fang, N. X.; Hammond, P. T.; Belcher, A. M. Tunable Localized Surface Plasmon-Enabled Broadband Light-Harvesting Enhancement for High-Efficiency Panchromatic Dye-Sensitized Solar Cells. *Nano Lett.* **2013**, *13*, 637−642.

(14) Jain, P. K.; El-Sayed, M. A. Plasmonic Coupling in Noble Metal Nanostructures. *Chem. Phys. Lett.* **2010**, *487*, 153−164.

(15) Webb, J. A.; Bardhan, R. Emerging Advances in Nanomedicine with Engineered Gold Nanostructures. *Nanoscale* **2014**, *6*, 2502−2530.

(16) Sonntag, M. D.; Klingsporn, J. M.; Zrimsek, A. B.; Sharma, B.; Ruvuna, L. K.; VanDuyne, R. P. Molecular Plasmonics for Nanoscale Spectroscopy. *Chem. Soc. Rev.* **2014**, *43*, 1230−1247.

(17) Catchpole, K. R.; Polman, A. Design Principles for Particle Plasmon Enhanced Solar Cells. *Appl. Phys. Lett.* **2008**, *93*, 191113.

(18) Hägglund, C.; Zäch, M.; Kasemo, B. Enhanced Charge Carrier Generation in Dye Sensitized Solar Cells by Nanoparticle Plasmons. *Appl. Phys. Lett.* **2008**, *92*, 013113.

(19) Westphalen, W.; Kreibig, U.; Rostalski, H.; Luth, H.; Meissner, D. Metal Cluster Enhanced Organic Solar Cells. *Sol. Energy Mater. Sol. C* **2000**, *61*, 97−105.

(20) Webb, J. A.; Erwin, W. R.; Zarick, H. F.; Aufrecht, J.; Manning, H.; Lang, M. J.; Pint, C. L.; Bardhan, R. Geometry Dependent Plasmonic Tunability and Photothermal Characteristics of Multi-branched Gold Nanoantennas. *J. Phys. Chem. C* **2014**, *118*, 3696−3707.

(21) Rycenga, M.; Xia, X.; Moran, C. H.; Zhou, F.; Qin, D.; Li, Z. Y.; Xia, Y. Generation of Hot Spots with Silver Nanocubes for Single-

Molecule Detection by Surface-Enhanced Raman Scattering. *Angew. Chem., Int. Ed.* **2011**, *50*, 5473−5477.
(22) Bardhan, R.; Grady, N. K.; Halas, N. J. Nanoscale Control of Near-Infrared Fluorescence Enhancement Using Au Nanoshells. *Small* **2008**, *4*, 1716−1722.
(23) Bantz, K. C.; Meyer, A. F.; Wittenberg, N. J.; Im, H.; Kurtulus, O.; Lee, S. H.; Lindquist, N. C.; Oh, S.-H.; Haynes, C. L. Recent Progress in SERS Biosensing. *Phys. Chem. Chem. Phys.* **2011**, *13*, 11551−11567.
(24) Brus, L. Noble Metal Nanocrystals: Plasmon Electron Transfer Photochemistry and Single-Molecule Raman Spectroscopy. *Acc. Chem. Res.* **2008**, *41*, 1742−1749.
(25) Qi, J.; Dang, X.; Hammond, P. T.; Belcher, A. M. Highly Efficient Plasmon-Enhanced Dye-Sensitized Solar Cells through Metal@Oxide Core-Shell Nanostructure. *ACS Nano* **2011**, *5*, 7108−7116.
(26) Naphade, R. A.; Tathavadekar, M.; Jog, J. P.; Agarkar, S.; Ogale, S. Plasmonic Light Harvesting of Dye Sensitized Solar Cells by Au-Nanoparticle Loaded TiO_2 Nanofibers. *J. Mater. Chem. A* **2014**, *2*, 975−984.
(27) Sheehan, S. W.; Noh, H.; Brudvig, G. W.; Cao, H.; Schmuttenmaer, C. A. Plasmonic Enhancement of Dye-Sensitized Solar Cells Using Core−Shell−Shell Nanostructures. *J. Phys. Chem. C* **2013**, *117*, 927−934.
(28) Jang, Y. H.; Jang, Y. J.; Kochuveedu, S. T.; Byun, M.; Lin, Z.; Kim, D. H. Plasmonic Dye-Sensitized Solar Cells Incorporated with Au-TiO_2 Nanostructures with Tailored Configurations. *Nanoscale* **2014**, *6*, 1823−1832.
(29) Haggui, M.; Dridi, M.; Plain, J.; Marguet, S.; Perez, H.; Schatz, G. C.; Wiederrecht, G. P.; Gray, S. K.; Bachelot, R. Spatial Confinement of Electromagnetic Hot and Cold Spots in Gold Nanocubes. *ACS Nano* **2012**, *6*, 1299−1307.
(30) Rycenga, M.; Kim, M. H.; Camargo, P. H.; Cobley, C.; Li, Z. Y.; Xia, Y. Surface-Enhanced Raman Scattering: Comparison of Three Different Molecules on Single-Crystal Nanocubes and Nanospheres of Silver. *J. Phys. Chem. A* **2009**, *113*, 3932−3939.
(31) Sau, T. K.; Murphy, C. J. Room Temperature, High-Yield Synthesis of Multiple Shapes of Gold Nanoparticles in Aqueous Solution. *J. Am. Chem. Soc.* **2004**, *126*, 8648−8649.
(32) Li, J. F.; Tian, X. D.; Li, S. B.; Anema, J. R.; Yang, Z. L.; Ding, Y.; Wu, Y. F.; Zeng, Y. M.; Chen, Q. Z.; Ren, B.; Wang, Z. L.; Tian, Z. Q. Surface Analysis Using Shell-Isolated Nanoparticle-Enhanced Raman Spectroscopy. *Nat. Protoc.* **2013**, *8*, 52−65.
(33) Baida, H.; Billaud, P.; Marhaba, S.; Christophilos, D.; Cottancin, E.; Crut, A.; Lerme, J.; Maioli, P.; Pellarin, M.; Broyer, M.; Del Fatti, N.; Vallee, F. Quantitative Determination of the Size Dependence of Surface Plasmon Resonance Damping in Single Ag@SiO_2 Nanoparticles. *Nano Lett.* **2009**, *9*, 3463−3469.
(34) Lin, S.-J.; Lee, K.-C.; Wu, J.-L.; Wu, J.-Y. Enhanced Performance of Dye-Sensitized Solar Cells via Plasmonic Sandwiched Structure. *Appl. Phys. Lett.* **2011**, *99*, 043306.
(35) Ding, I. K.; Zhu, J.; Cai, W.; Moon, S.-J.; Cai, N.; Wang, P.; Zakeeruddin, S. M.; Grätzel, M.; Brongersma, M. L.; Cui, Y.; McGehee, M. D. Plasmonic Dye-Sensitized Solar Cells. *Adv. Energy Mater.* **2011**, *1*, 52−57.